

www.acsabm.org Article

Design of Curcumin Loaded Carbon Nanodots Delivery System: Enhanced Bioavailability, Release Kinetics, and Anticancer Activity

Durga M. Arvapalli, Alex T. Sheardy, Kokougan Allado, Harish Chevva, Ziyu Yin, and Jianjun Wei*



Cite This: ACS Appl. Bio Mater. 2020, 3, 8776–8785



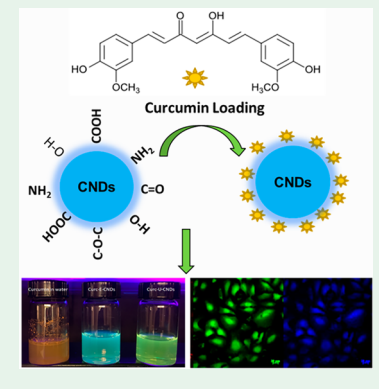
ACCESS

Metrics & More



Supporting Information

ABSTRACT: Despite the potential health benefits of curcumin, such as antioxidant, anticancer, anti-inflammatory, and antimicrobial properties, its usage is limited by poor bioavailability and low aqueous solubility. Nano-formulations of curcumin have gained a lot of attention due to their increased bioavailability, solubility, circulation times, targeted specificity, decreased biodegradation, better stability, and improved cellular uptake. The current study aimed to enhance the bioavailability of curcumin using carbon nanodots (CNDs) as loading vehicles to deliver curcumin due to their excellent biocompatibility, aqueous solubility, and photoluminescence properties. Two types of CNDs (E-CNDs and U-CNDs) were used for curcumin loading and characterized for particle size, morphology, loading capability (measured as adsorption efficiency and loading capacity), stability, photoluminescence properties, in vitro drug release studies, cellular uptake, and anticancer activity. The prepared curcumin-loading CNDs (Curc-CNDs) displayed sizes around or below 10 nm with good stability. The Curc-E-CNDs demonstrated a curcumin adsorption efficiency of 91% in solution, while the Curc-U-CNDs have an adsorption efficiency of 82%. Both have a loading capacity of 3.4—3.8% with



respect to the weight of the CNDs. Curcumin release followed a controlled sustained pattern that a total of 60% and 74% of curcumin was released at 72 h from Curc-E-CNDs and Curc-U-CNDs, respectively, in pH 5 buffer, and almost 90% was released in culture media within 96 h. Both of the Curc-CNDs were uptaken by cells and exhibited prominent cytotoxicity toward cancer cells. The results clearly depict the role of CNDs as efficient carriers for curcumin delivery with prolonged release and enhanced bioavailability, thereby improving the overall antitumor activity.

KEYWORDS: carbon nanodots, curcumin, anticancer, nano-formulations, cellular uptake, cytotoxicity

■ INTRODUCTION

Curcumin, a natural polyphenolic spice obtained from the tropical southeast Asian plant *Curcuma longa* (turmeric), has applications that date back centuries as a dietary supplement, with its anti-inflammatory, analgesic, antiseptic, and antioxidant properties. Phase I clinical trials in humans showed no side effects upon administration of curcumin (8 g/day). Curcumin can inhibit cell cycle progression, induce apoptosis, and halt cell proliferation process in cancer cell lines, thereby establishing its potential role as an antitumor agent. However, the poor bioavailability, low aqueous solubility, poor absorption, rapid degradation, fast metabolism, and systemic elimination hinder this elixir drug's usage as a chemotherapeutic agent. Moreover, the intracellular uptake of curcumin is limited by its hydrophobicity, where curcumin binds to the lipids of the cell membrane without entering the cytoplasm.

Structural and chemical modifications have been implemented to increase the bioavailability of curcumin, but are limited due to the low potency of the derivates compared to the native curcumin, therefore requiring higher doses to elicit therapeutic responses. ^{16,17} Nanobased drug delivery systems have emerged as an eminent solution to overcome the

limitations and increase the bioavailability and targetability of curcumin, thereby improving the overall anticancer activity. ¹⁸ Nanoparticle size, shape, and surface chemistry plays an important role in the selection of drug delivery vehicles for cancer therapy. ¹⁹ Various nanoformulation based drug delivery systems such as liposomes, ^{20–23} polymeric nanoparticles, ^{24,25} and hydrogels ^{26,27} showed promising curcumin delivery, however they also exhibit some drawbacks. Specifically, use of liposomes is limited by low drug entrapment and instability, ²⁸ polymeric nanoparticles offer toxicity of unreacted monomers and initial burst release of curcumin, respectively. ²⁹ Adsorption of curcumin onto soluble nanoparticles improves the solubility and stability of the hydrophobic drugs, which overcomes rapid drug metabolism, transports the drug to the target sites, and reduces adverse side effects. ³⁰

Received: September 9, 2020 Accepted: October 29, 2020 Published: November 11, 2020





© 2020 American Chemical Society

Carbon nanodots (CNDs) are spherical low molecular weight luminescent particles (<10 nm) with excellent photostability against photobleaching, and possess tunable emission spectra, photoelectric activities, ^{31,32} good biocompatibility, ³³ and low toxicity. ^{34–36} These desirable properties of the CNDs opened up several applications in photocatalysis, ³⁷ biosensing, ³⁸ bioimaging, ^{39,40} and anti- or pro-oxidation. ^{41–44} While tremendous progress has been made in designing drug carrying nanovehicles for cancer therapy, ^{45–49} relatively less light has been shed on the CNDs. ^{50–53} Due to their superior chemical and physical properties, CNDs with large numbers of surface functional groups offer high surface area for drug loading, thereby increasing the solubility of hydrophobic drugs which can be used as drug-loading vehicles to reach cancer sites with better targeting and delivery efficiency, thereby reducing the side effects and improving drug tolerance.

This work reports on the synthesis of curcumin-loading CNDs (Curc-CNDs) with enhanced bioavailability and anticancer property of curcumin along with incorporating the CNDs' features, such as photoluminescence, small size (~5 nm), and stability for highly efficient cellular uptake and delivery tracking by imaging. In the present study, two types of CNDs (E-CNDs and U-CNDs) are functionalized with curcumin for examining the bioavailability and eliciting the therapeutic effects. The two CNDs have different surface functional groups, surface charge, and size distribution, but both are soluble in water and have good biocompatibility. This comparative study is focused on understanding how these differences impact on curcumin loading and releasing. The results may provide guidance in the design of CNDs and the application for drug delivery. Specifically, the Curc-CNDs were characterized regarding the structure, composite and optical properties. Curcumin release kinetics from the complex was investigated using the Korsmeyer and Peppas equation. The kinetics studies provide information about the pH dependent release of curcumin as a function of time. Intracellular and anticancer activities of Curc-CNDs were tested in two cancer cell lines, HepG2 and A549 cells, and one normal cell line, EA. hy926. Curcumin loading onto the CNDs increases the bioavailability in cells compared to native curcumin, thereby meeting the low concentrations required to elicit anticancer effects.

EXPERIMENTAL SECTION

Materials. Citric acid (ACROS Organics), ethylenediamine, urea (Fisher Scientific), curcumin (Chem Cruz), phosphate buffer solution (PBS) (Life Tech), quinine sulfate dihydrate, methanol (Fisher Scientific), AS49 cell line, HepG2 cell line, EA. hy926 cell line, DMEM (Dulbecco's minimum essential medium), EMEM (Eagle's minimum essential medium), and F12 K (Ham's F-12K (Kaighn's) Medium), (ATCC), pen/strep solution, tryplE, fetal bovine serum and CCK-8 assay kit (Sigma-Aldrich), and Alamar blue (Thermo Scientific).

Synthesis of CNDs. E-CNDs and U-CNDs were synthesized as mentioned in our previous work. ³⁷ Briefly, E-CNDs were prepared by dissolving 960 mg of citric acid in 1 mL each of DI water and ethylene diamine (EDA). The mixture was pyrolyzed by a 300 W microwave (CEM Corp 908005 Microwave Reactor) for 18 min at a temperature below 150 °C. The resulting brown foamy solution was dissolved in 5 mL of DI water for purification. U-CNDs were prepared by pyrolyzing urea (1 g) and citric acid (1 g) in 1 mL of DI water at 110 °C for 12 min at 150 W power. Large aggregated particles were removed by centrifugation. Both samples were purified by dialysis against DI water (1000 MWCO), and solid powders were obtained by lyophilization.

Curcumin Loading. The synthesized E-CNDs and U-CNDs were loaded with curcumin. Briefly, curcumin was dissolved in methanol (1:1 w/v), and the solution was added dropwise to either E-CNDs or U-CNDs at a concentration of 2 mg/mL. The reactant mixture was ultrasonicated in a water bath for 20 min and shaken on rotary shaker (500 rpm) overnight at room temperature. The methanol was evaporated using rotary evaporation and the Curc-CNDs were centrifuged. The pellet was dissolved in a known amount of methanol and quantified using UV-vis spectrophotometer (Varian Cary 6000i) at 425 nm. A curcumin standard curve was plotted with known concentrations. The adsorption efficiency is defined as the amount of drug entrapped/adsorbed onto the CNDs to the total amount of drug added, whereas the loading capacity expresses the amount of curcumin loading per unit weight of the CNDs. The curcumin adsorption efficiency and loading capacity in percentage are calculated using the formula as follows:

$$AE \% = \frac{TCA - FCS}{TCA} \times 100$$
 (1)

$$LC\% = \frac{\text{wt of curcumin loaded onto CNDs}}{\text{wt of CNDs}} \times 100$$

where AE is the adsorption efficiency, TCA is the total curcumin added, FCS is the free curcumin in solution, LC% is the loading capacity, and wt is weight.

Physicochemical Properties and Characterization. Atomic Force Microscopy (Agilent 5600LS AFM), Transmission Electron Microscopy (TEM, Carl Zeiss Libra 120 Plus), and zeta potentiometer (Malvern Zetasizer ZEN3600) were used for the determination of the size and charge of the CNDs before and after functionalization with Curcumin, respectively. The samples were analyzed by FT-IR spectroscopy (Agilent FTIR) to identify the functional groups of curcumin in the functionalized Curc-CNDS. Chemical structure and elemental composition of the Curc-CNDs were characterized using XPS (Thermo Scientific ESCALAB Xi⁺) and Raman spectroscopy (Horiba XploRA One Raman Confocal Microscope System), respectively. Ultraviolet-visible spectrophotometry (Varian Cary 6000i) and fluorescence spectrophotometry (Varian Cary Eclipse) were used to investigate the optical properties of the Curc-CNDs, respectively. The fluorescence quantum yield (QY) of the CNDs before and after curcumin functionalization was determined using Quinine Sulfate (QS) as a standard fluorescent compound in 0.1 M H₂SO₄ using the following equation: ^{54,5}

$$\Phi_{\rm C} = \Phi_{\rm QS} \times \frac{\rm GradC}{\rm GradQS} \times \frac{\eta_{\rm C}^2}{\eta_{\rm QS}^2}$$
(3)

where Φ represents the quantum yield, Grad is the gradient from the plot of integrated fluorescence intensity vs absorbance, and η is the refractive index (aqueous solution 1.33). The subscript QS and C denoted quinine sulfate and CNDs before and after functionalization with curcumin, respectively.

pH Dependent Release Kinetics. The Curc-CNDs were dissolved in 10 mM PBS and incubated at 37 °C at a pH of 5 and 7. Samples were taken at different time intervals (0, 0.5, 1, 2, 4, 8, 16, 24, 48, and 72 h) and centrifuged for 3 min at 1200 rpm to pelletize released curcumin. Concentrations of released curcumin were calculated from the curcumin standard curve. Curcumin release studies were also carried out in cell culture media to determine the release pattern. The release % was calculated using the following formula:

release % =
$$\left(\frac{\text{curcumin released}}{\text{total curcumin in CNDs}}\right) \times 100$$
 (4)

The release pattern of the curcumin was analyzed using the formulation derived by Korsmeyer and Peppas to analyze the release pattern of drugs, which is given by the following:

$$M_t/M_{\infty} = kt^n \tag{5}$$

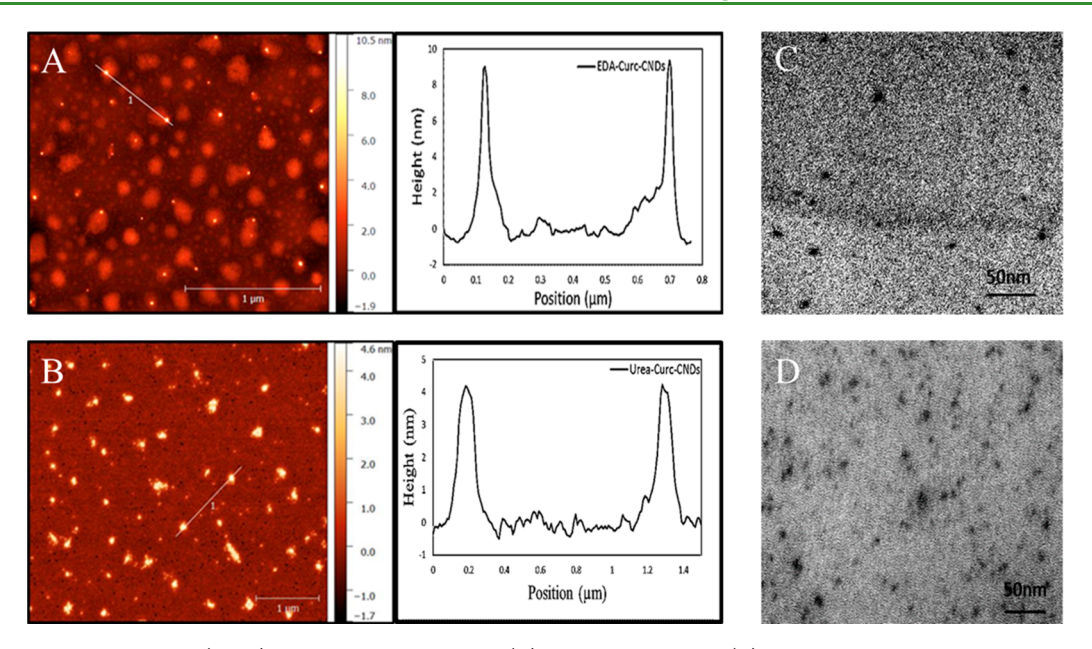


Figure 1. Atomic force microscopy (AFM) images of Curc-E-CNDs (A) and Curc-U-CNDs (B) with their respective height profiles around 9 and 4 nm respectively, and the TEM images of Curc-E-CNDs (C) and Curc-U-CNDs (D), respectively.

$$Log(M_t/M_{\infty}) = Log k + n Log t \tag{6}$$

where, M_t and M_{∞} are the fraction of drug released at time t and infinite time, respectively, k is a kinetic constant, and n is the release exponent, indicative of transport mechanism of drug. ⁵⁶

Cell Culture. HepG2 cells (human hepatocellular cancer cells) were maintained in EMEM supplemented with 10% FBS and 1% pen/strep antibiotic solution, A549 cells (adenocarcinomic human alveolar basal epithelial cells) were maintained in F12K media supplemented with 10% FBS and 1% pen/strep antibiotic solution and EA. hy926 cells were maintained in DMEM media supplemented with 10% FBS and 1% pen/strep antibiotic solution. All the cells were kept in an incubator with 5% $\rm CO_2$ at 37 °C.

Biocompatibility of the CNDs. The biocompatibility of E-CNDs, U-CNDs and Curc-CNDs were determined using CCK-8 assay. The assay is based on the conversion of WST-8 [2-(2-methoxy-4-nitrophenyl)-3-(4-nitrophenyl)-5-(2,4disulfophenyl)-2H-tetrazolium, monosodium salt] dye to a water-soluble orange colored formazan complex due to the cellular dehydrogenase activity. The cell viability is measured at an optical density of 450 nm. ⁵⁷ The EA. hy926 cells were preseded in 96-well plate overnight and starved in low serum media for 24 h. The respective medium with different concentrations of the CNDs and Curc-CNDs (0, 0.1, 0.2, 0.4, 0.8, 1.6, and 3.2 mg/mL) were added to investigate their biocompatibility toward both the cancerous cells and the normal cells incubated for 24 h. Viability of the cells was examined by measuring absorption at 450 nm after 1 h. The equation used for calculating viability % is as follows:

viability % =
$$[(OD_{sample} - OD_{blank})/(OD_{control} - OD_{blank})] \times 100$$
 (7)

In Vitro Therapeutic Effect of Curc-CNDs. 10,000 cells of HepG2 and A549 were preseded in a 96-well plate overnight and starved in low serum media for 24 h. Different concentrations (0, 0.1, 0.2, 0.4, 0.8, 1.6, and 3.2 mg/mL) of the CNDs and Curc-CNDs were added to HepG2 and A549 cells and incubated for 24 h. Viability was determined using Alamar blue assay and % of living cells was calculated using the above-mentioned formula.

Intracellular Uptake and Cytotoxicity of Curc-CNDs. Live/Dead assay were conducted on HepG2 and A549 cells. Cells (1×10^5) were seeded on coverslips that were placed in 12 well plates overnight. The medium was replaced with different concentrations (0, 0.4, 0.8, and, 1.6 mg/mL) of Curc-E-CNDs and Curc-U-CNDs and

incubated for 12 h. The growth medium was replaced with live dead reagent (calcein AM and ethidium homodimer-1) dissolved in sterile phosphate buffer saline (PBS), and incubated for 45 min. The cells were washed thrice with PBS, and the coverslip was placed on the slide. The cells were imaged under a confocal microscope (Zeiss Z1 Spinning Disk Confocal Microscope) for intracellular localization of the Curc-E-CNDs. The images were collected at 20× magnification. The live cells uptake calcein AM and stain green, whereas the dead cells uptake ethidium homodimer-1 and stain red.

Statistical Analysis. All data were expressed as mean \pm standard error. Each experiment was repeated in triplicates and significance was analyzed by multifactor analysis of variance (ANOVA) with accepted statistical significance at a level of p < 0.05.

■ RESULTS AND DISCUSSION

Characterization of Curc-CNDs. The successful conjugation of CNDs with curcumin was validated using different characterization techniques. The AFM images of Curc-E-CNDs (Figure 1A) and Curc-U-CNDs (Figure 1B) showed an even dispersion with average height of 9 and 4 nm,

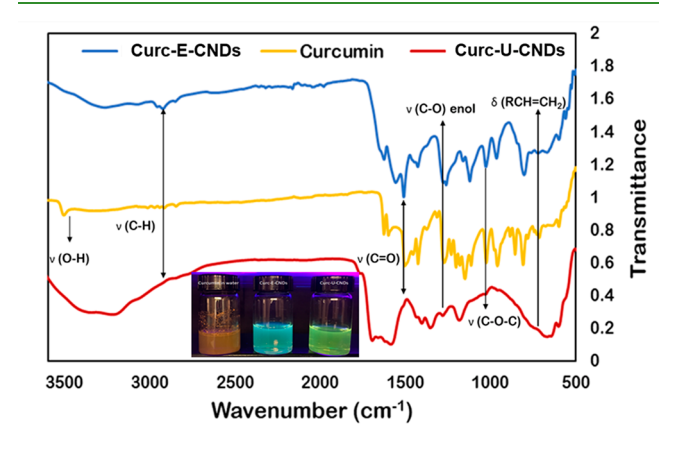


Figure 2. FTIR spectra of Curc-E-CNDs, curcumin, and Curc-U-CNDs with their characteristic peaks. Inset is an optical image of curcumin, Curc-E-CNDs, and Curc-UCNDs in water solution. Insoluble pure curcumin is observed in water.

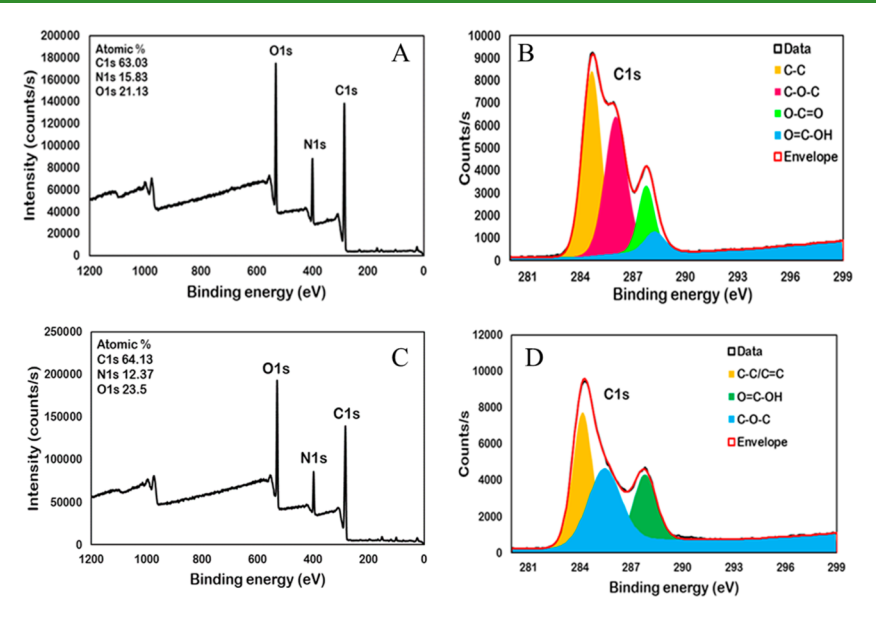


Figure 3. XPS survey spectra of Curc-E-CNDs (A) and Curc-U-CNDs (C). High resolution C 1s (B, D) XPS spectra of Curc-E-CNDs and Curc-U-CNDs, respectively.

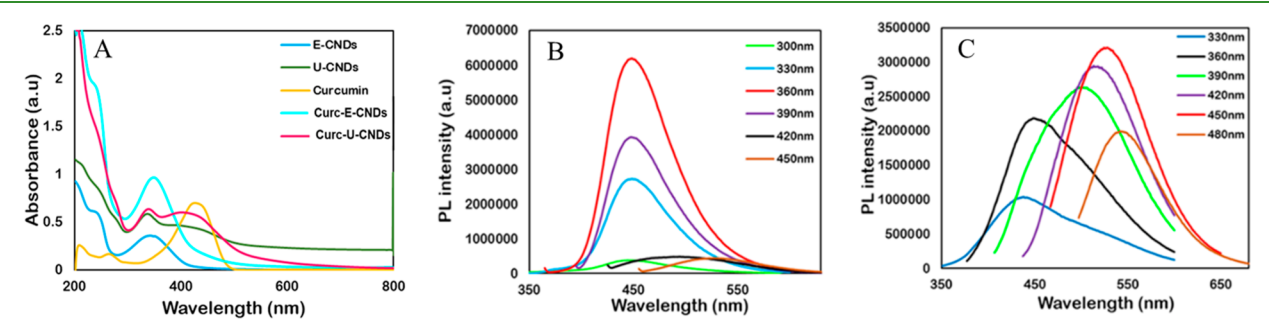


Figure 4. UV—vis absorption spectra of E-CNDs, U-CNDs, curcumin, Curc-E-CNDs, and Curc-U-CNDs (A). Excitation dependent fluorescence spectra of Curc-E-CNDs (0.5 mg/mL) (B) and Curc-U-CNDs (0.5 mg/mL) (C), respectively.

respectively. Since the radius of curvature of the AFM probe is larger compared to both the Curc-CNDs, only the height data can be used to determine the size. The average diameter of the curcumin functionalized Curc-E-CNDs (Figure 1C) and Curc-U-CNDs (Figure 1D) is around 10 and 5 nm, respectively, from the TEM images, which is in accordance with the AFM data. The zeta potential of E-CNDs is -7.32 ± 0.9 mV, and upon functionalization with curcumin changed to -11.7 ± 1.3 mV at a physiological pH of 7.4, in good agreement with nanoformulated curcumin (-13.8 mV) reported by Dende et al.⁵⁸ Upon functionalization of U-CNDs with curcumin, the zeta potential has changed from -38.5 ± 2.7 mV to $-32.9 \pm$ 3.8 mV. The measured zeta potential of curcumin dissolved in methanol is -15.2 ± 4.9 mV (Figure S1 of the Supporting Information, SI). The zeta potential of Curc-E-CNDs shifts positively while that of the Curc-U-CNDs shifts negatively. The zeta potential shift can be interpreted by the hydrogen bonding and electrostatic interactions between curcumin and CNDs. Structure characterization of E-CNDs suggests the presence of a greater fraction of amine groups and fewer carboxylic acids while the U-CNDs possess a greater fraction of carboxylic acids than amines,³⁸ and thus a more negative zeta potential of U-CNDs than the E-CNDs at pH 7.4. This means the U-CNDs can act primarily as hydrogen bond acceptors due to the deprotonated carboxylates. The protonated amines on the E-CND surface can act as hydrogen bond donors. The

ketone and hydroxyl groups in curcumin may shield the functional groups by hydrogen bonding, thus changing the zeta potential. Specifically, the curcumin molecules shield some carboxylates in the U-CNDs, resulting in a positive move in zeta potential; while the protonated amines in the E-CNDs are partially neutralized, thus obtaining a more negative zeta potential. These analyses also suggest that the hydrogen bond interactions are one of the driving forces for the curcumin loading to the CNDs, in addition to the electrostatic interactions. 59,60 Nevertheless, the zeta potential changes observed in both the Curc-CNDs and AFM visualization of particle size increase corroborate the successful adsorption of curcumin onto the CNDs. The higher negative zeta potential indicates better stability in aqueous solution.⁶¹ This property should allow for a longer circulation time of the Curc-U-CNDs in the tumor microenvironment.⁶²

While curcumin is not well dissolved in water, the Curc-ECNDs and Curc-UCNDs form homogeneous solution in water (inset in Figure 2). The FTIR analysis further confirmed the functionalization of the CNDs with curcumin. Native curcumin exhibits characteristic peaks at 3509, 3024, 1624, and 1275 cm⁻¹ which correspond to OH stretching of phenol, CH stretching, C=O, C=C stretching mode, and C-O enol stretching, respectively. Both E-CNDs and U-CNDs, after functionalization with curcumin, exhibit similar characteristic peaks to that of curcumin confirming the successful

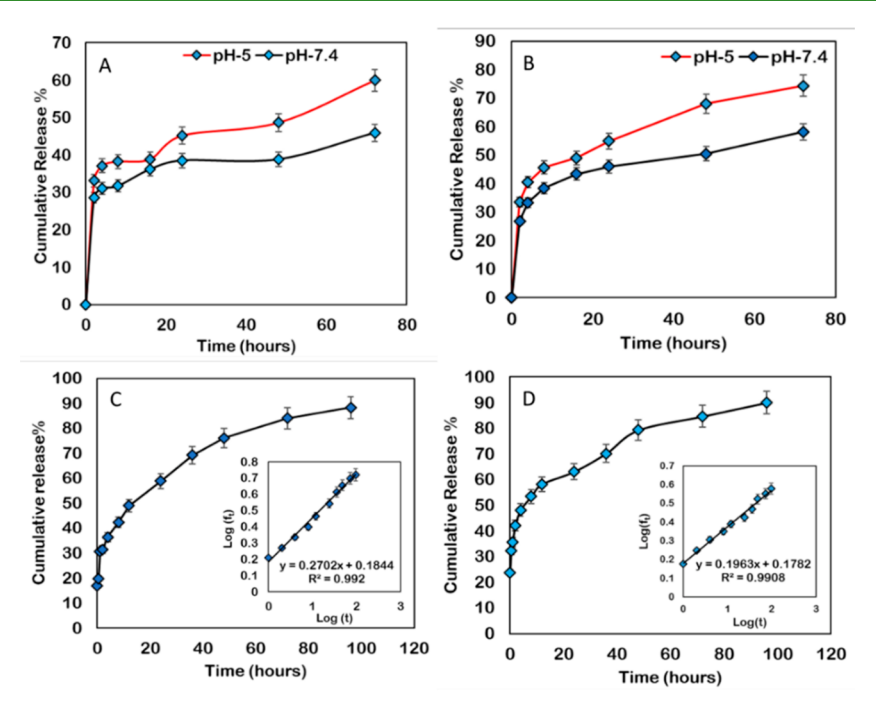


Figure 5. Curcumin release profile of Curc-E-CNDs (A) and Curc-U-CNDs (B) under two different pH-5 and 7.4 in PBS and Curc-E-CNDs (C) and Curc-U-CNDs (D) in EMEM media. Inserts in (C) and (D) are Korsmeyer-Peppas release model of Curcumin. All the data values were done in triplicates with mean \pm SDs.

conjugation of CNDs and curcumin (Figure 2). Moreover, the O–H and N–H stretching of the E-CNDs and U-CNDs is conserved in the Curc-CNDs after functionalization (Figure S2).³⁸ Raman spectra of both CNDs show the increase in D band intensity after functionalization with curcumin, which can be attributed to the carbon atoms excited from sp² to sp³ hybridization due to the introduction of oxygenated functional groups (Figure S3).⁶⁴

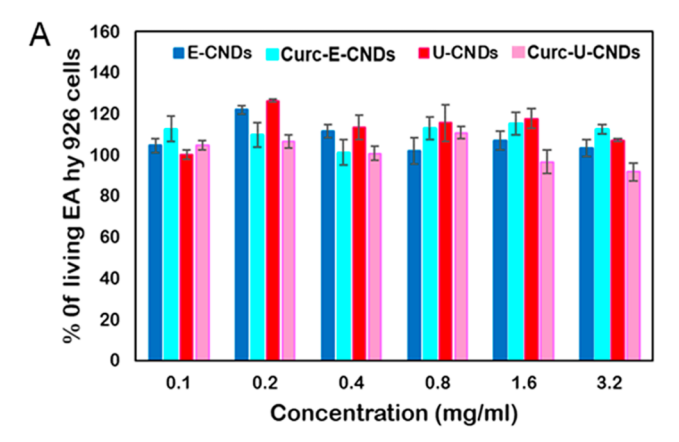
XPS spectrum of curcumin depicts the presence of two elements carbon at 285.0 eV and oxygen at 532.0 eV, respectively (Figure S4A). The XPS spectra of both E-CNDs (Figure 3A) and U-CNDs (Figure 3C) after functionalization with curcumin show the presence of carbon, nitrogen, and oxygen at 285.0, 400.5, and 532.0 eV. The curve fitting C 1s spectra of Curc-E-CNDs (Figure 3B) and Curc-U-CNDs (Figure 3D) have chemical states at corresponding to C-C, C-O-C, O-C=O and O=C-OH, similar to that of the curcumin C 1s spectra (Figure S4). Similarly, the C 1s characteristic peaks of E-CNDs and U-CNDs are conserved after functionalization with curcumin (Figure S5). 56 The additional peak O=C-OH is observed in both the types of CNDs after functionalization with curcumin (Figure 3B,D). The O 1s spectra of Curc-E-CNDs depicts O-H and C=O peaks (Figure S6A) and Curc-U-CNDs have presented peaks corresponding to O-H and O-C=O (Figure S6C), whereas the individual high resolution N 1s spectra of both the Curc-E-CNDs (Figure S6B) and Curc-U-CNDs (Figure S6D) show the presence of C-N-C and N-H peaks.

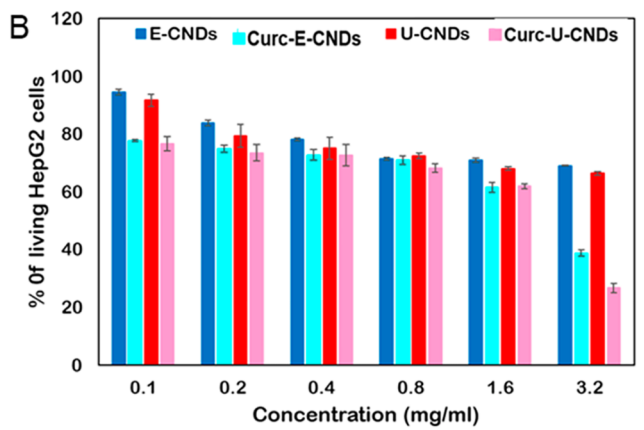
In UV-vis (Figure 4A), E-CNDs and U-CNDs have shoulder peaks located at 250 and 245 nm which are attributed to π - π * transitions of C=C (aromatic sp² domains). The E-CNDs and U-CNDs show strong broad peaks at 350 and 337 nm, respectively, which are assigned to n- π transitions of C=O bond involving functional groups with electron lone pairs. The UV-vis spectrum of curcumin shows two distinct peaks at ~268 nm and ~426 nm corresponding to n- π * and π - π *

transitions, respectively (Figure 4A).⁶⁵ The UV—vis spectrum of Curc-E-CNDs depicts strong peak at 356 nm and shoulder peak at 240 nm, respectively. Curc-U-CNDs exhibit two peaks at 343 and 427 nm (Figure 4A). The excitation dependent behavior at different excitation wavelengths gives information about the strong emission peaks. Curc-E-CNDs (Figure 4B) and Curc-U-CNDs (Figure 4C) exhibited strong emission peaks at an excitation wavelength of 360 and 450 nm, respectively. Unlike curcumin, both Curc-CNDs are readily dispersed in water and exhibited good fluorescence stability over a time period of 50 days (Figure S7). The quantum yields of the Curc-E-CNDs (48.74%) and Curc-U-CNDs (6.54%) are calculated with reference to quinine sulfate (Table S1).

Curcumin Loading and Release. The curcumin adsorption efficiency and loading capacity for Curc-E-CNDs were determined to be 91.5 \pm 1.5% and 3.8 \pm 0.8% and for Curc-U-CNDs to be 81.9 \pm 1.9% and 3.4 \pm 0.6%, respectively. These results demonstrate good loading capability of both CNDs. In E-CNDs, more nitrogen containing groups exist than that in U-CNDs from the XPS characterization. Since curcumin has negativity in solution and thus it is not surprising that the E-CNDs present a little higher loading capability due to the stronger hydrogen bond and electrostatic interactions with ketone and hydroxyl groups of curcumin because of more amine groups. ^{59,60}

The curcumin release pattern of both the Curc-CNDs was first studied in PBS at two different pH (7.4 and 5) over a time course of 72 h. High curcumin release (%) is observed at a pH 5 in a gradual controlled manner for both the Curc-CNDs (Figure 5A,B). The enhanced drug release at pH 5 may be due to weaker interactions of Curcumin and CNDs in acidic environment because of the protonation of both carboxylates and amines resulted weak hydrogn bond and electrostatic interactions. This is beneficial for curcumin to elicit its therapeutic effects in the tumor microenvironment at acidic pH. Slow release rate of curcumin in solution of pH 7.4 can be





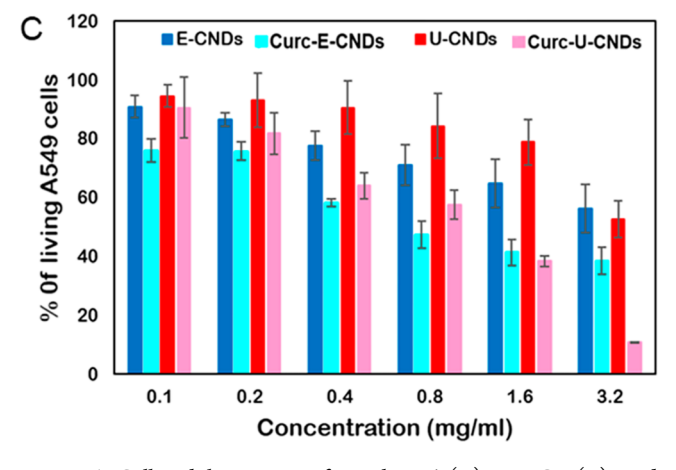


Figure 6. Cell viability assays of EA. hy926 (A), HepG2 (B), and A549 (C) cells treated with different concentrations of E-CNDs & Curc-E-CNDs and U-CNDs & Curc-U-CNDs for 24 h.

attributed to the stronger association between CNDs and curcumin because of more deprotonated carboxylates and amines than in pH 5. Initial curcumin burst release of Curc-E-CNDs and Curc-U-CNDs was found to be 33.1% and 33.5%, respectively, at 2 h at pH 5 using curcumin standard curve (Figure S8), which might be due to the desorption and release of surface curcumin into the surrounding media. Thereafter, the curcumin release from both the Curc-CNDs followed a controlled sustained release pattern which can be attributed to the lipophilic nature of curcumin (Figure 5). A total of 59.9% and 74.3% of curcumin was released at 72 h from Curc-E-CNDs and, Curc-U-CNDs, respectively. The slower release of curcumin from Curc-E-CNDs can be exlained by the stronger interactions between the E-CNDs and curcumin, consistent

with the loading capability of curcumin. The loading and release analysis suggests that manipulating the surface functional groups of CNDs can tune the drug loading capability and release rate at different pH solutions.

The drug release behavior was further studied by fitting the curcumin release with kinetic models. The curcumin release data were plotted using Korsmeyer and Peppas equation with R^2 values of 0.98–0.99 and n values below 0.45 for both the types of Curc CNDs at pH of 5 and 7.4 (Figures S9 and S10). The n values less than 0.45 (n < 0.45) confirms the fickian diffusion of the solute molecule (curcumin) from Curc-CNDs complex into the surrounding media due to chemical gradient. A similar release trend is observed when the Curc CNDs are suspended in EMEM cell culture media, with n values less than 0.45 (Figure 5C–D). Almost 90% of curcumin is released into the media within 96 h.

Cell Viability. Biocompatibility of the CNDs and Curc-CNDs were analyzed using CCK-8viability assay for the normal cell line EA. hy926. The cells showed no significant signs of cellular toxicity on treatment with the CNDs and Curc-CNDs even at high concentration of 3.2 mg/mL (Figure 6A). In concert, HepG2 and A549 cells were treated with CNDs and Curc-CNDs at concentrations of 0.1, 0.2, 0.4, 0.8, 1.6, and 3.2 mg/mL for 24 h. The number of viable cells decreased in Curc CNDs treated HepG2 and A549 cells in comparison to the CNDs treated cells (Figure 6B-C) from the alamar blue assay. At a concentration of 3.2 mg/mL, the cell viability is around 40% and 30% for the HepG2 cells treated with Curc-E-CNDs and Curc-U-CNDs (Figure 6B), respectively. A549 cells displayed a cell viability of ~38% and ~18% when treated with Curc-E-CNDs and Curc-U-CNDs (Figure 6C) at a maximum concentration of 3.2 mg/mL for 24 h, respectively. A more rapid decrease in the number of viable cells is observed in both the cells treated with Curc-U-CNDs in comparison to Curc-E-CNDs (Figure 6C). The A549 cell viability assay was carried out for an extended period of 48 and 72 h to observe the effects of Curc-CNDs on cell viabilty. Curc-E-CNDs treated cells show a cell viability of ~30% and ~25%, while Curc-U-CNDs depict ~5% and ~2% at a concentration of 3.2 mg/mL, at time period of 48 and 72 h, respectively (Figure S11). Cancer cells treated with the Curc-CNDs showed cytotoxicity due to the higher uptake and release of curcumin compared to normal cells. This might be attributed to membrane structure and protein composition differences and low pH in the cells.⁶⁶ The presence of high levels of glutathione in tumor cells enhances the sensitivity of tumor cells to curcumin. 67 Upon treatment with Curc-CNDs, both HepG2 and A549 cells showed dose-dependent increase in cellular toxicity; and the high cellular toxicity of the Curc-U-CNDs can be attributed to the more release of curcumin, which was observed from the release profile. The mechanism of cytotoxicity of curcumin in cancer cells is dependent on the type of cancer being treated. Specifically, in liver cancer cell lines curcumin suppress tumor cell survival and proliferation through inhibition of NF-kB signaling pathway. 68 Whereas in lung cancer cells, curcumin inhibits cell prolifeartion and induces apoptosis through suppression of PI3K/Akt signaling pathway.6

Cellular Uptake and Cytotoxicity of Curc-CNDs. The cellular uptake studies of Curc-E-CNDs and Curc-U-CNDs were conducted using two cell lines HepG2 and A549 at concentrations of 0.4, 0.8, and, 1.6 mg/mL. Both types of Curc-CNDs show good cellular uptake in HepG2 and A549

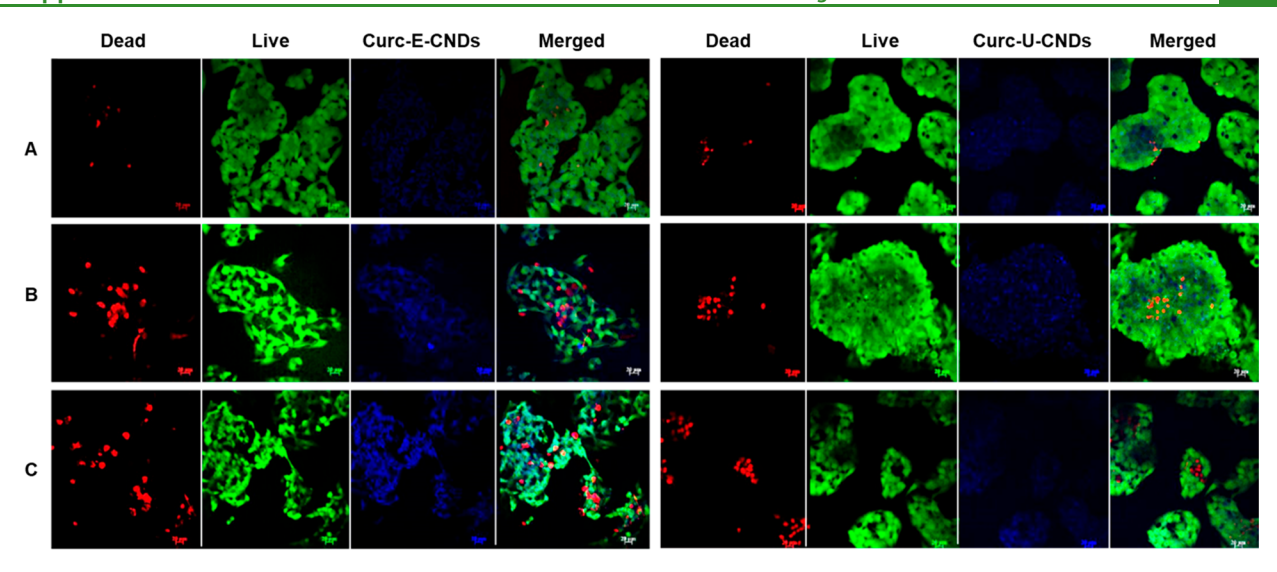


Figure 7. Fluorescence images of live and dead HepG2 cells incubated with Curc-E-CNDs and Curc-U-CNDs at different concentrations (0.4 (A), 0.8 (B), and 1.6 (C) mg/mL) for 12 h.

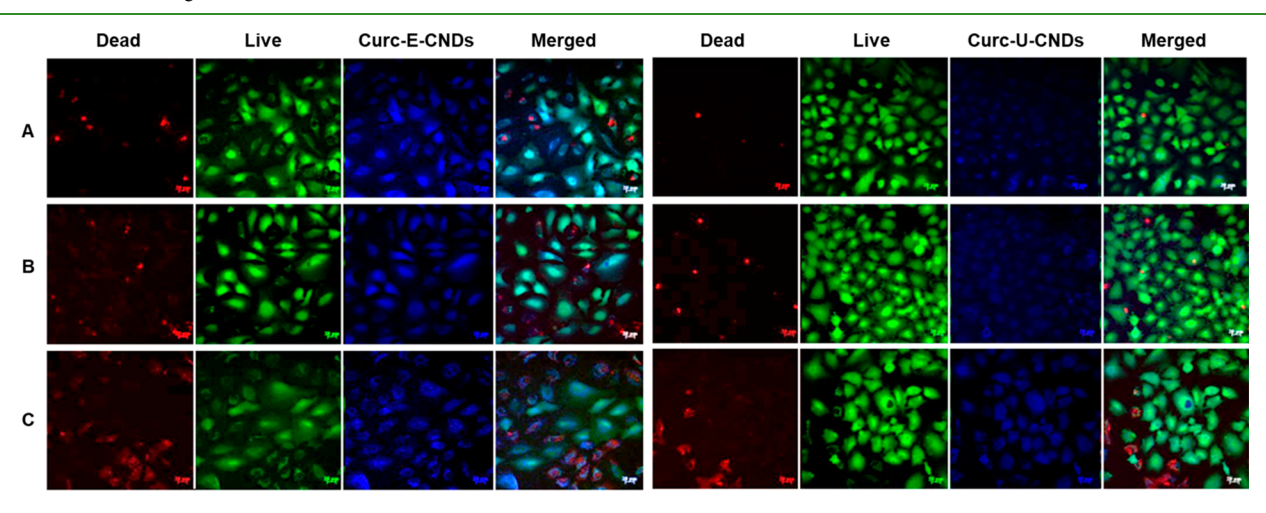


Figure 8. Fluorescence images of live and dead A549 cells incubated with Curc-E-CNDs & Curc-U-CNDs at different concentrations (0.4 (A), 0.8 (B), and 1.6 (C) mg/mL) for 12 h.

cells. Cells treated with Curc-E-CNDs exhibited high fluorescence intensity compared to Curc-U-CNDs (Figures 7 and 8), which is due to the high quantum yield of E-CNDs.³⁸

The cellular toxicity of Curc-CNDs was evaluated using live dead assay in two cell lines HepG2 and A549. Curc-CNDs exhibited cytotoxicity in a dose-dependent manner in both cell types. As the concentration of Curc-CNDs was increased, the number of dead cells increased gradually. At a concentration of 1.6 mg/mL, both Curc-CNDs showed a significant decrease in the number of viable cells (Figures 7 and 8) and A549 cells showed change in the cell morphology (Figure 8C). 3.2 mg/ mL concentration was also tested, but the cells were all detached from the coverslip after the treatment, due to the toxicity at high concentration. The fluorescent microscopy images show Curc-CNDs are found to be distributed both in cytoplasm and nucleus (Figures 7 and 8). With increase in concentration of Curc-CNDs, the cellular toxicity increased along with cellular uptake which is evident from live/dead assay. The results of more of curcumin localized in the cells might induce dose dependent DNA damage to nuclear as well as mitochondrial genome with increase of ROS levels and lipid peroxidation.70

CONCLUSIONS

In the current study, Curcumin loaded CNDs were prepared in an cost-effective manner, to enhance the bioavailability of curcumin and explore the antiproliferative effects of encapsulated curcumin. The characterization studies confirmed the successful conjugation of curcumin with CNDs with overall small size, high loading capacity, good photoluminescence properties, and stability. The curcumin release studies have shown better release of curcumin in solution with pH-5, inferring more amount of drug delivered tumor microenvironment compared to normal tissues. The CNDs used for curcumin loading are shown to be nontoxic to normal cells, thereby proving a better vehicle for curcumin delivery. Curc-U-CNDs have shown enhanced cellular toxicity even at low concentrations which is further supported by the zeta potential measurements (longer circulation times) and drug release profile of curcumin and can be attributed to the effective loading of curcumin onto the functional group rich CNDs. In conclusion, the CNDs can be valuable vehicles for curcumin delivery with enhanced bioavailability, small size, high loading capability, better photoluminescence, and biocompatibility, eliciting improved anticancer properties at low concentrations.

ASSOCIATED CONTENT

Supporting Information

The Supporting Information is available free of charge at https://pubs.acs.org/doi/10.1021/acsabm.0c01144.

FTIR spectra, Raman spectra, XPS survey spectrum, fluorescence stability and quantum yield, curcumin standard curve, curcumin release model, and cell viability up to 72 h treatment (PDF)

AUTHOR INFORMATION

Corresponding Author

Jianjun Wei — Department of Nanoscience, Joint School of Nanoscience and Nanoengineering, University of North Carolina at Greensboro, Greensboro, North Carolina 27401, United States; orcid.org/0000-0002-2658-0248; Phone: 1-336-285-2859; Email: j_wei@uncg.edu

Authors

- Durga M. Arvapalli Department of Nanoscience, Joint School of Nanoscience and Nanoengineering, University of North Carolina at Greensboro, Greensboro, North Carolina 27401, United States
- Alex T. Sheardy Department of Nanoscience, Joint School of Nanoscience and Nanoengineering, University of North Carolina at Greensboro, Greensboro, North Carolina 27401, United States
- Kokougan Allado Department of Nanoscience, Joint School of Nanoscience and Nanoengineering, University of North Carolina at Greensboro, Greensboro, North Carolina 27401, United States
- Harish Chevva Department of Nanoscience, Joint School of Nanoscience and Nanoengineering, University of North Carolina at Greensboro, Greensboro, North Carolina 27401, United States
- Ziyu Yin Department of Nanoscience, Joint School of Nanoscience and Nanoengineering, University of North Carolina at Greensboro, Greensboro, North Carolina 27401, United States

Complete contact information is available at: https://pubs.acs.org/10.1021/acsabm.0c01144

Author Contributions

The manuscript was written with contributions by all authors. All authors have approved the final version of the manuscript.

Funding

The authors acknowledge the financial support from the US National Science Foundation (NSF) (Award no.: 1832134), and a North Carolina State fund through the Joint School of Nanoscience and Nanoengineering (JSNN), a joint institution between The University of North Carolina—Greensboro and North Carolina A&T State University.

Notes

The authors declare no competing financial interest.

ACKNOWLEDGMENTS

The research was conducted at the Joint School of Nanoscience and Nanoengineering, a member of Southeastern Nanotechnology Infrastructure Corridor (SENIC) and National Nanotechnology Coordinated Infrastructure (NNCI), which is supported by the National Science Foundation (ECCS-1542174).

REFERENCES

- (1) Shishodia, S.; Sethi, G.; Aggarwal, B. B. Curcumin: getting back to the roots. *Ann. N. Y. Acad. Sci.* **2005**, *1056*, 206–17.
- (2) Wilken, R.; Veena, M. S.; Wang, M. B.; Srivatsan, E. S. Curcumin: A review of anti-cancer properties and therapeutic activity in head and neck squamous cell carcinoma. *Mol. Cancer* **2011**, *10*, 12.
- (3) Rao, C. V.; Rivenson, A.; Simi, B.; Reddy, B. S. Chemoprevention of colon carcinogenesis by dietary curcumin, a naturally occurring plant phenolic compound. *Cancer Res.* **1995**, *55* (2), 259–266.
- (4) Gupta, S. C.; Patchva, S.; Aggarwal, B. B. Therapeutic roles of curcumin: lessons learned from clinical trials. *AAPS J.* **2013**, *15* (1), 195–218.
- (5) Moos, P. J.; Edes, K.; Mullally, J. E.; Fitzpatrick, F. A. Curcumin impairs tumor suppressor p53 function in colon cancer cells. *Carcinogenesis* **2004**, 25 (9), 1611–7.
- (6) Choudhuri, T.; Pal, S.; Das, T.; Sa, G. Curcumin selectively induces apoptosis in deregulated cyclin D1-expressed cells at G2 phase of cell cycle in a p53-dependent manner. *J. Biol. Chem.* **2005**, 280 (20), 20059–68.
- (7) Hassan, F.-U.; Rehman, M. S.-U.; Khan, M. S.; Ali, M. A.; Javed, A.; Nawaz, A.; Yang, C. Curcumin as an Alternative Epigenetic Modulator: Mechanism of Action and Potential Effects. *Front. Genet.* **2019**, *10*, 514.
- (8) Huminiecki, L.; Horbanczuk, J.; Atanasov, A. G. The functional genomic studies of curcumin. *Semin. Cancer Biol.* **2017**, *46*, 107–118.
- (9) Kunnumakkara, A. B.; Bordoloi, D.; Padmavathi, G.; Monisha, J.; Roy, N. K.; Prasad, S.; Aggarwal, B. B. Curcumin, the golden nutraceutical: multitargeting for multiple chronic diseases. *Br. J. Pharmacol.* **2017**, *174* (11), 1325–1348.
- (10) Mirzaei, H.; Khoi, M. J.; Azizi, M.; Goodarzi, M. Can curcumin and its analogs be a new treatment option in cancer therapy? *Cancer Gene Ther.* **2016**, 23 (11), 410.
- (11) Panda, A. K.; Chakraborty, D.; Sarkar, I.; Khan, T.; Sa, G. New insights into therapeutic activity and anticancer properties of curcumin. *J. Exp. Pharmacol.* **2017**, *9*, 31–45.
- (12) Kundu, M.; Sadhukhan, P.; Ghosh, N.; Chatterjee, S.; Manna, P.; Das, J.; Sil, P. C. pH-responsive and targeted delivery of curcumin via phenylboronic acid-functionalized ZnO nanoparticles for breast cancer therapy. *J. Adv. Res.* **2019**, *18*, 161–172.
- (13) Anand, P.; Kunnumakkara, A. B.; Newman, R. A.; Aggarwal, B. B. Bioavailability of curcumin: problems and promises. *Mol. Pharmaceutics* **2007**, *4* (6), 807–18.
- (14) Barry, J.; Fritz, M.; Brender, J. R.; Smith, P. E.; Lee, D. K.; Ramamoorthy, A. Determining the effects of lipophilic drugs on membrane structure by solid-state NMR spectroscopy: the case of the antioxidant curcumin. *J. Am. Chem. Soc.* **2009**, *131* (12), 4490–8.
- (15) Tsukamoto, M.; Kuroda, K.; Ramamoorthy, A.; Yasuhara, K. Modulation of raft domains in a lipid bilayer by boundary-active curcumin. *Chem. Commun.* **2014**, *50* (26), 3427–3430.
- (16) Tomeh, M. A.; Hadianamrei, R.; Zhao, X. A Review of Curcumin and Its Derivatives as Anticancer Agents. *Int. J. Mol. Sci.* **2019**, 20 (5), 1033.
- (17) Shoji, M.; Nakagawa, K.; Watanabe, A.; Tsuduki, T.; Yamada, T.; Kuwahara, S.; Kimura, F.; Miyazawa, T. Comparison of the effects of curcumin and curcumin glucuronide in human hepatocellular carcinoma HepG2 cells. *Food Chem.* **2014**, *151*, 126–32.
- (18) Gera, M.; Sharma, N.; Ghosh, M.; Huynh, D. L.; Lee, S. J.; Min, T.; Kwon, T.; Jeong, D. K. Nanoformulations of curcumin: an emerging paradigm for improved remedial application. *Oncotarget* **2017**, 8 (39), 66680–66698.
- (19) Davis, M. E.; Chen, Z. G.; Shin, D. M. Nanoparticle therapeutics: an emerging treatment modality for cancer. *Nat. Rev. Drug Discovery* **2008**, 7 (9), 771–82.
- (20) Wang, D.; Veena, M. S.; Stevenson, K.; Tang, C.; Ho, B.; Suh, J. D.; Duarte, V. M.; Faull, K. F.; Mehta, K.; Srivatsan, E. S.; Wang, M. B. Liposome-encapsulated curcumin suppresses growth of head and neck squamous cell carcinoma in vitro and in xenografts through the

- inhibition of nuclear factor kappaB by an AKT-independent pathway. Clin. Cancer Res. 2008, 14 (19), 6228-36.
- (21) Karewicz, A.; Bielska, D.; Loboda, A.; Gzyl-Malcher, B.; Bednar, J.; Jozkowicz, A.; Dulak, J.; Nowakowska, M. Curcumin-containing liposomes stabilized by thin layers of chitosan derivatives. *Colloids Surf.*, B **2013**, *109*, 307–16.
- (22) Li, C.; Zhang, Y.; Su, T.; Feng, L.; Long, Y.; Chen, Z. Silicacoated flexible liposomes as a nanohybrid delivery system for enhanced oral bioavailability of curcumin. *Int. J. Nanomed.* **2012**, *7*, 5995–6002.
- (23) Li, L.; Braiteh, F. S.; Kurzrock, R. Liposome-encapsulated curcumin: in vitro and in vivo effects on proliferation, apoptosis, signaling, and angiogenesis. *Cancer* **2005**, *104* (6), 1322–31.
- (24) Rejinold, N. S.; Yoo, J.; Jon, S.; Kim, Y. C. Curcumin as a Novel Nanocarrier System for Doxorubicin Delivery to MDR Cancer Cells: In Vitro and In Vivo Evaluation. *ACS Appl. Mater. Interfaces* **2018**, *10* (34), 28458–28470.
- (25) Bisht, S.; Feldmann, G.; Soni, S.; Ravi, R.; Karikar, C.; Maitra, A.; Maitra, A. Polymeric nanoparticle-encapsulated curcumin ("nanocurcumin"): a novel strategy for human cancer therapy. *J. Nanobiotechnol.* **2007**, *5*, 3.
- (26) Liu, J.; Chen, Z.; Wang, J.; Li, R.; Li, T.; Chang, M.; Yan, F.; Wang, Y. Encapsulation of Curcumin Nanoparticles with MMP9-Responsive and Thermos-Sensitive Hydrogel Improves Diabetic Wound Healing. ACS Appl. Mater. Interfaces 2018, 10 (19), 16315–16326.
- (27) Altunbas, A.; Lee, S. J.; Rajasekaran, S. A.; Schneider, J. P.; Pochan, D. J. Encapsulation of curcumin in self-assembling peptide hydrogels as injectable drug delivery vehicles. *Biomaterials* **2011**, 32 (25), 5906–5914.
- (28) Sharma, A.; Sharma, U. S. Liposomes in drug delivery: Progress and limitations. *Int. J. Pharm.* **1997**, *154* (2), 123–140.
- (29) Hatefi, A.; Amsden, B. Biodegradable injectable in situ forming drug delivery systems. *J. Controlled Release* **2002**, 80 (1), 9–28.
- (30) Yallapu, M. M.; Nagesh, P. K.; Jaggi, M.; Chauhan, S. C. Therapeutic Applications of Curcumin Nanoformulations. *AAPS J.* **2015**, *17* (6), 1341–56.
- (31) Zeng, Z.; Zhang, W.; Arvapalli, D. M.; Bloom, B.; Sheardy, A.; Mabe, T.; Liu, Y.; Ji, Z.; Chevva, H.; Waldeck, D. H.; Wei, J. A fluorescence-electrochemical study of carbon nanodots (CNDs) in bio- and photoelectronic applications and energy gap investigation. *Phys. Chem. Chem. Phys.* **2017**, *19* (30), 20101–20109.
- (32) Sheardy, A. T.; Arvapalli, D. M.; Wei, J. Experimental and Time-Dependent Density Functional Theory Modeling Studies on the Optical Properties of Carbon Nanodots. *J. Phys. Chem. C* **2020**, 124 (8), 4684–4692.
- (33) Baker, S.; Baker, G. Luminescent Carbon Nanodots: Emergent Nanolights. *Angew. Chem., Int. Ed.* **2010**, *49*, 6726–44.
- (34) Sun, Y.-P.; Zhou, B.; Lin, Y.; Wang, W.; Fernando, K. A. S.; Pathak, P.; Meziani, M. J.; Harruff, B. A.; Wang, X.; Wang, H.; Luo, P. G.; Yang, H.; Kose, M. E.; Chen, B.; Veca, L. M.; Xie, S.-Y. Quantum-Sized Carbon Dots for Bright and Colorful Photoluminescence. *J. Am. Chem. Soc.* **2006**, *128* (24), *7756*–7757.
- (35) Wang, Q.; Huang, X.; Long, Y.; Wang, X.; Zhang, H.; Zhu, R.; Liang, L.; Teng, P.; Zheng, H. Hollow luminescent carbon dots for drug delivery. *Carbon* **2013**, *59*, 192–199.
- (36) Ji, Z.; Yin, Z.; Jia, Z.; Wei, J. Carbon Nanodots Derived from Urea and Citric Acid in Living Cells: Cellular Uptake and Antioxidation Effect. *Langmuir* **2020**, *36* (29), 8632–8640.
- (37) Cao, L.; Sahu, S.; Anilkumar, P.; Bunker, C. E.; Xu, J.; Fernando, K. A. S.; Wang, P.; Guliants, E. A.; Tackett, K. N.; Sun, Y.-P. Carbon Nanoparticles as Visible-Light Photocatalysts for Efficient CO₂ Conversion and Beyond. *J. Am. Chem. Soc.* **2011**, *133* (13), 4754–4757.
- (38) Arvapalli, D. M.; Sheardy, A. T.; Alapati, K. C.; Wei, J. High Quantum Yield Fluorescent Carbon Nanodots for detection of Fe (III) Ions and Electrochemical Study of Quenching Mechanism. *Talanta* **2020**, 209, 120538.

- (39) Cao, L.; Wang, X.; Meziani, M. J.; Lu, F.; Wang, H.; Luo, P. G.; Lin, Y.; Harruff, B. A.; Veca, L. M.; Murray, D.; Xie, S.-Y.; Sun, Y.-P. Carbon Dots for Multiphoton Bioimaging. *J. Am. Chem. Soc.* **2007**, 129 (37), 11318–11319.
- (40) Yang, S.-T.; Cao, L.; Luo, P. G.; Lu, F.; Wang, X.; Wang, H.; Meziani, M. J.; Liu, Y.; Qi, G.; Sun, Y.-P. Carbon Dots for Optical Imaging in Vivo. *J. Am. Chem. Soc.* **2009**, *131* (32), 11308–11309.
- (41) Zhang, W.; Zeng, Z.; Wei, J. Electrochemical Study of DPPH Radical Scavenging for Evaluating the Antioxidant Capacity of Carbon Nanodots. *J. Phys. Chem. C* **2017**, *121* (34), 18635–18642.
- (42) Zhang, W.; Chavez, J.; Zeng, Z.; Bloom, B.; Sheardy, A.; Ji, Z.; Yin, Z.; Waldeck, D. H.; Jia, Z.; Wei, J. Antioxidant Capacity of Nitrogen and Sulfur Codoped Carbon Nanodots. *ACS Appl. Nano Mater.* **2018**, *1* (6), 2699–2708.
- (43) Ji, Z.; Sheardy, A.; Zeng, Z.; Zhang, W.; Chevva, H.; Allado, K.; Yin, Z.; Wei, J. Tuning the Functional Groups on Carbon Nanodots and Antioxidant Studies. *Molecules* **2019**, *24* (1), 152.
- (44) Ji, Z.; Arvapalli, D. M.; Zhang, W.; Yin, Z.; Wei, J. Nitrogen and sulfur co-doped carbon nanodots in living EA.hy926 and A549 cells: oxidative stress effect and mitochondria targeting. *J. Mater. Sci.* **2020**, 55, 6093–6104.
- (45) Cho, H. S.; Dong, Z.; Pauletti, G. M.; Zhang, J.; Xu, H.; Gu, H.; Wang, L.; Ewing, R. C.; Huth, C.; Wang, F.; Shi, D. Fluorescent, superparamagnetic nanospheres for drug storage, targeting, and imaging: a multifunctional nanocarrier system for cancer diagnosis and treatment. ACS Nano 2010, 4 (9), 5398–404.
- (46) Cho, H.-Y.; Mavi, A.; Chueng, S.-T. D.; Pongkulapa, T.; Pasquale, N.; Rabie, H.; Han, J.; Kim, J. H.; Kim, T.-H.; Choi, J.-W.; Lee, K.-B. Tumor Homing Reactive Oxygen Species Nanoparticle for Enhanced Cancer Therapy. ACS Appl. Mater. Interfaces 2019, 11 (27), 23909–23918.
- (47) Sztandera, K.; Gorzkiewicz, M.; Klajnert-Maculewicz, B. Gold Nanoparticles in Cancer Treatment. *Mol. Pharmaceutics* **2019**, *16* (1), 1–23.
- (48) El-Sawy, H. S.; Al-Abd, A. M.; Ahmed, T. A.; El-Say, K. M.; Torchilin, V. P. Stimuli-Responsive Nano-Architecture Drug-Delivery Systems to Solid Tumor Micromilieu: Past, Present, and Future Perspectives. ACS Nano 2018, 12 (11), 10636–10664.
- (49) Taghavi, S.; Abnous, K.; Taghdisi, S. M.; Ramezani, M.; Alibolandi, M. Hybrid carbon-based materials for gene delivery in cancer therapy. *J. Controlled Release* **2020**, *318*, 158–175.
- (50) Kong, T.; Hao, L.; Wei, Y.; Cai, X.; Zhu, B. Doxorubicin conjugated carbon dots as a drug delivery system for human breast cancer therapy. *Cell Proliferation* **2018**, *51* (5), e12488.
- (51) Hettiarachchi, S. D.; Graham, R. M.; Mintz, K. J.; Zhou, Y.; Vanni, S.; Peng, Z.; Leblanc, R. M. Triple conjugated carbon dots as a nano-drug delivery model for glioblastoma brain tumors. *Nanoscale* **2019**, *11* (13), 6192–6205.
- (52) Feng, T.; Ai, X.; An, G.; Yang, P.; Zhao, Y. Charge-Convertible Carbon Dots for Imaging-Guided Drug Delivery with Enhanced in Vivo Cancer Therapeutic Efficiency. ACS Nano 2016, 10 (4), 4410–4420
- (53) Yuan, Y.; Guo, B.; Hao, L.; Liu, N.; Lin, Y.; Guo, W.; Li, X.; Gu, B. Doxorubicin-loaded environmentally friendly carbon dots as a novel drug delivery system for nucleus targeted cancer therapy. *Colloids Surf., B* **2017**, *159*, 349–359.
- (54) Heller, C. A.; Henry, R. A.; McLaughlin, B. A.; Bliss, D. E. Fluorescence spectra and quantum yields. Quinine, uranine, 9,10-diphenylanthracene, and 9,10-bis(phenylethynyl)anthracenes. *J. Chem. Eng. Data* 1974, 19 (3), 214–219.
- (55) Zhu, S.; Meng, Q.; Wang, L.; Zhang, J.; Song, Y.; Jin, H.; Zhang, K.; Sun, H.; Wang, H.; Yang, B. Highly Photoluminescent Carbon Dots for Multicolor Patterning, Sensors, and Bioimaging. *Angew. Chem., Int. Ed.* **2013**, 52 (14), 3953–3957.
- (56) Korsmeyer, R. W.; Gurny, R.; Doelker, E.; Buri, P.; Peppas, N. A. Mechanisms of solute release from porous hydrophilic polymers. *Int. J. Pharm.* **1983**, *15* (1), 25–35.
- (57) Cai, L.; Qin, X.; Xu, Z.; Song, Y.; Jiang, H.; Wu, Y.; Ruan, H.; Chen, J. Comparison of Cytotoxicity Evaluation of Anticancer Drugs

- between Real-Time Cell Analysis and CCK-8 Method. ACS Omega 2019, 4 (7), 12036–12042.
- (58) Dende, C.; Meena, J.; Nagarajan, P.; Nagaraj, V. A.; Panda, A. K.; Padmanaban, G. Nanocurcumin is superior to native curcumin in preventing degenerative changes in Experimental Cerebral Malaria. *Sci. Rep.* **2017**, *7* (1), 10062.
- (59) Yang, P.; Zhu, Z.; Zhang, T.; Zhang, W.; Chen, W.; Cao, Y.; Chen, M.; Zhou, X. Orange-Emissive Carbon Quantum Dots: Toward Application in Wound pH Monitoring Based on Colorimetric and Fluorescent Changing. *Small* **2019**, *15* (44), 1902823.
- (60) Lin, C.-J.; Chang, L.; Chu, H.-W.; Lin, H.-J.; Chang, P.-C.; Wang, R. Y. L.; Unnikrishnan, B.; Mao, J.-Y.; Chen, S.-Y.; Huang, C.-C. Antiviral Carbon Dots: High Amplification of the Antiviral Activity of Curcumin through Transformation into Carbon Quantum Dots. *Small* **2019**, *15* (41), 1970219.
- (61) Terence. Colloid Science Principles, 2nd ed.; Wiley: New York, 2010
- (62) Alexis, F.; Pridgen, E.; Molnar, L. K.; Farokhzad, O. C. Factors affecting the clearance and biodistribution of polymeric nanoparticles. *Mol. Pharmaceutics* **2008**, *5* (4), 505–15.
- (63) Muthoosamy, K.; Abubakar, I. B.; Bai, R. G.; Loh, H.-S.; Manickam, S. Exceedingly Higher co-loading of Curcumin and Paclitaxel onto Polymer-functionalized Reduced Graphene Oxide for Highly Potent Synergistic Anticancer Treatment. *Sci. Rep.* **2016**, *6* (1), 32808.
- (64) Hussain, S.; Shah, K. A.; Islam, S. S. Investigation of effects produced by chemical functionalization in single-walled and multi-walled carbon nanotubes using Raman spectroscopy. *Mater. Sci.-Pol.* **2013**, *31* (2), 276–280.
- (65) Jagannathan, R.; Abraham, P. M.; Poddar, P. Temperature-Dependent Spectroscopic Evidences of Curcumin in Aqueous Medium: A Mechanistic Study of Its Solubility and Stability. *J. Phys. Chem. B* **2012**, *116* (50), 14533–14540.
- (66) Kunwar, A.; Barik, A.; Mishra, B.; Rathinasamy, K.; Pandey, R.; Priyadarsini, K. I. Quantitative cellular uptake, localization and cytotoxicity of curcumin in normal and tumor cells. *Biochim. Biophys. Acta, Gen. Subj.* **2008**, *1780* (4), 673–679.
- (67) Syng-ai, C.; Kumari, A. L.; Khar, A. Effect of curcumin on normal and tumor cells: Role of glutathione and bcl-2. *Mol. Cancer Ther.* **2004**, 3 (9), 1101.
- (68) Marquardt, J. U.; Gomez-Quiroz, L.; Arreguin Camacho, L. O.; Pinna, F.; Lee, Y. H.; Kitade, M.; Dominguez, M. P.; Castven, D.; Breuhahn, K.; Conner, E. A.; Galle, P. R.; Andersen, J. B.; Factor, V. M.; Thorgeirsson, S. S. Curcumin effectively inhibits oncogenic NF-kappaB signaling and restrains stemness features in liver cancer. *J. Hepatol.* 2015, 63 (3), 661–9.
- (69) Wang, M.; Jiang, S.; Zhou, L.; Yu, F.; Ding, H.; Li, P.; Zhou, M.; Wang, K. Potential Mechanisms of Action of Curcumin for Cancer Prevention: Focus on Cellular Signaling Pathways and miRNAs. *Int. J. Biol. Sci.* **2019**, *15* (6), 1200–1214.
- (70) Cao, J.; Jia, L.; Zhou, H.-M.; Liu, Y.; Zhong, L.-F. Mitochondrial and Nuclear DNA Damage Induced by Curcumin in Human Hepatoma G2 Cells. *Toxicol. Sci.* **2006**, *91* (2), 476–483.